scientific reports

Check for updates

OPEN

Bio-combustion synthesis of silver nanoparticles and evaluation of their effective antibacterial and photodegradation properties

Sanjay S. Majani[1], K. B. Ramesh[2], Bharath K. Devendra[3], Poojitha B. Sridhara Setty[4], Pallavi Singh[5], Muzaffar Iqbal[6], Kasim Sakran Abass[7], Chandan Shivamallu[8], Raghavendra G. Amachawadi[9], Victor Stupin[10], Ekaterina Silina[11]✉ & Shiva Prasad Kollur[1]✉

The green chemistry approach in synthesizing nanoparticles, particularly using plant extract, has gained booming demand for eco-friendly nanotechnology, evaluating their multifunctional properties, and exploring potential applications. Hence, addressing the need for sustainable nanomaterials in biomedical and environmental fields. This work describes the synthesis of silver nanoparticles (AgNPs) using *Manilkara zapota (M. zapota)* leaf extract as a reducing agent through a simple bio-combustion method. The synthesized AgNPs were characterized by various analytical techniques such as UV-visible spectroscopy, powder X-ray diffraction (PXRD), scanning electron microscopy (SEM), transmission electron microscopy (TEM), and so on. The optical studies of the AgNPs reveal a bandgap energy of about 3.31 eV. The nanoparticles synthesized in this work were found to crystallize in a cubic phase, corresponding to JCPDS #96-9013046, in the Fm-3 m space group. The crystallite size was 22.38 nm and was independently confirmed through the W-H plot (24.75 nm). Infrared spectroscopy results revealed the characteristics of O-H stretching at 3335 cm^{-1} and a metal peroxide peak at 849 cm^{-1}, respectively. It was seen that the SEM and TEM images depict a clustered agglomeration of the nanoparticles, while EDAX confirmed the elemental composition. The as-synthesized AgNPs showed high catalytic efficiency towards degradation of MB dye (83.33%) following 0th order kinetics with an R^2 value of 0.98 and rate constant k_0 of 0.007, under acidic conditions at pH-2 being optimal for their performance. The antibacterial assays showed that AgNPs were effective against both *Staphylococcus aureus* (gram-positive) and *Escherichia coli* (gram-negative) bacterial strains. Activity was observed at a low concentration of 400 µg/mL. Hence, the obtained AgNPs prepared via bio-combustion route resulted in a potential multifunctional nanomaterial with strong catalytic properties coupled with antibacterial activity.

Keywords Antibacterial activity, Bio-Combustion synthesis, *M. zapota*, SDG 6, Silver nanoparticles

Science has continued to advance at a fast pace, an aspect valid by the observation of nanotechnology, which is embarking on a phenomenal growth in the development of new products with multifunctional applications inherent in them and, in equal measure, applied in the field of medicine and environmental conservation[1–4].

[1]School of Physical Sciences, Amrita Vishwa Vidyapeetham, Mysuru Campus, Mysuru, Karnataka 570 026, India. [2]Department of Chemistry, SSK Basaveshwar UG & PG College, Basavakalyana, Affiliated to Bidar University, Bidar, Karnataka 585 327, India. [3]Department of Chemistry, M. S. Ramaiah College of Arts, Science and Commerce, MSR Nagar, MSRIT Post, Bengaluru, Karnataka 560 054, India. [4]Department of Biotechnology, GM University, Davangere, Karnataka 577 006, India. [5]Department of Biotechnology, Graphic Era Deemed to be University, Dehradun, Uttarakhand 248 002, India. [6]Department of Pharmaceutical Chemistry, College of Pharmacy, King Saud University, Riyadh 11451, Saudi Arabia. [7]Department of Physiology, Biochemistry, and Pharmacology, College of Veterinary Medicine, University of Kirkuk, Kirkuk 36001, Iraq. [8]Department of Biotechnology and Bioinformatics, JSS Academy of Higher Education and Research, Mysuru, Karnataka 570 015, India. [9]Department of Clinical Sciences, College of Veterinary Medicine, Kansas State University, Manhattan, KS 66506–5606, USA. [10]Department of Surgery, Pirogov Russian National Research Medical University, 117997 Moscow, Russia. [11]Institute of Digital Biodesign and Modeling of Living Systems, I.M. Sechenov First Moscow State Medical University (Sechenov University), 119991 Moscow, Russia. ✉email: silinaekaterina@mail.ru; shivachemist@gmail.com

Metal nanoparticles, with their intriguing physicochemical properties, have played a significant role in the technological advancement of nanotechnology. Nonetheless, finding eco-friendly and cost-effective materials and synthesis procedures is a significant problem, which has driven increased interest in green technologies[5,6]. Among all these materials, the silver nanoparticles (AgNPs) have such great interest owing to their enhanced bactericidal, antifungal, and catalytic properties as well as other physicochemical properties[7–10]. Earlier, AgNPs synthesis has been carried out by chemical and physical methods, which are expensive, time-consuming, energy consuming and involve toxic reducing agents, raising certain environmental and safety concerns. To these challenges, the green synthesis approach using bio-sources, including plants, fungi, and bacteria, has therefore emerged as the best and safest way of preparing nanoparticles[11,12]. Considering the biogenic sources for the synthesis of nano silver, the *Manilkara zapota (M. zapota)* could be more effective for green synthesis of AgNPs[13–15]. This tree-borne fruit is native to Mexico and Central America and is widely grown globally for the edible nuts as well as medicinal values due to the existence of phytochemicals like tannins, flavonoids, saponins, and other bioactive compounds[16]. Such phytochemicals have antioxidant, antimicrobial, and anti-inflammatory properties; therefore, *M. zapota* can be considered a renewable bio-template for synthesizing functional nanomaterials[17,18]. *M. zapota* is considered bioactive, so it enhances this property to synthesize AgNPs and follow the green chemistry strategy to minimize the negative impact of nanoparticles on the environment.

The biosynthesis of AgNPs using the plant extract of *M. zapota* belongs to the biogenic category, whereby there is a reduction of Ag^{+} to AgO. The process is generally carried out under slightly acidic pH, and the process does not involve the use of toxic solvents or other such chemicals. This results in the synthesis of AgNPs, which are entrapped by capping agents; these are other phytochemicals that are present in the plant extract that assist in preventing the coagulation of the nanoparticles[19,20]. This is a fast method when it comes to nanoparticle synthesis since it is cheaper and yields nanoparticles with properties pegged to the phytochemicals present in the plant extract. The bio-assisted combustion with calcination approach of synthesizing nanomaterials has a significant advantage over standard, environmentally friendly synthesis in that it allows for the rapid, energy-efficient synthesis of highly crystalline nanoparticles with regulated shape. Optimized calcination at 750 °C eliminates residual organics and promotes crystallinity without particle aggregation, enhancing the functional qualities of the nanomaterial[21–23].

The biomedical applicability of AgNPs is widely recognized and documented in various studies, which emphasize their effectiveness against many pathogens such as bacteria, fungi, and viruses. The activity of AgNPs as antimicrobials has been ascribed to the ability to generate reactive oxygen species (ROS), destroy microbial cell membranes, and interfere with essential metabolic processes in these cells. Nevertheless, depending on the size, shape, surface charge, and capping agents on nanoparticles that depend on the synthesis method and the reducing agent being used, their action mechanisms differ[24–26].

There has been an increasing interest in the recent past on using plant-mediated AgNPs for environmental applications, particularly in degrading organic pollutants. Among the most stubborn and harmful chemicals that are in use in the textile, paper, and leather industries are organic dyes that persist in wastewater[27–29]. In developing effective and sustainable wastewater treatment tools, a lot of research has been directed towards the catalytic degradation of these dyes with AgNPs. The capacity of AgNPs to initiate the disintegration of organic dyes is largely reliant upon their surface area, electronic configuration, and presence of active sites, which can be tailored by controlling the synthesis method and capping agents used[30,31]. Herein lies a double advantage of using *M. zapota* L. extract for the biosynthesis of AgNPs. First, new antibacterial agents could be made by exploiting the antimicrobial properties of *M. zapota*-mediated AgNPs, especially at such times when there happens to be a rise in antibiotic resistance levels. Second, these nanoparticles can work as catalysts for breaking down dangerous organic dyes, hence providing an eco-friendly technique for removing environmental pollutants.

The present work novels on evaluating the multifunctional potency of synthesized AgNPs through a green approach. The prepared AgNPs were characterized using various physicochemical techniques for structure, optical, and morphological properties. Further, the bio-combusted sample is employed in degrading the cationic dye, Methylene Blue (MB). The results were utilized in studying the kinetics and mechanism involved in degrading the same. Furthermore, the same has been utilized in anti-bacterial evaluation against Gram-positive and Gram-negative bacterial strains.

Experimental

Chemicals and analytical techniques

The pristine analytical grade silver nitrate ($AgNO_3$) (≥ 99.0%), purchased from Sigma-Aldrich (USA), was used as a precursor. The Bruker D8 Advance Powder X-ray diffractometer (Microstar Proteum 8) was used as an experimental method of examining the structure of the as-synthesized sample (). Moreover, the FESEM JEOL JSM-7100 F device was utilized to determine the surface morphology and elemental composition of the samples. The precisely resolved JOEL JEM-2100 plus TEM Japanese Transmission Electron Microscope was employed to give a more accurate average particle size assessment utilizing ImageJ, a free software available at https://imagej.net/ij/index.html. The spectrophotometer employed in probing the band gap and conducting photocatalysis was Lab India UV-3200. FTIR analysis was performed using SHIMADZU IR, XRoss. Horiba nanoparticle analyzer SZ-100 was employed for Dynamic Light Scattering (DLS) analysis.

Preparation of *M. zapota* L. extract

The preparation of *M. zapota L.* extract follows the method reported in our previous work[40]. The *M. zapota* leaves were identified with the help of a taxonomist (Dr. Murali, University of Mysore), and fresh leaves were plucked from the plant in the botanical garden located at Manasagangotri campus, University of Mysore (deposited in the Herbarium lab at University of Mysore having voucher number 12/1941). The leaves were properly cleansed with double-distilled water and placed in a beaker measuring 250 milliliters along with 100 mL of water. The

mixture was heated for an extended period until 100 mL was reduced to 25 mL of the leaf extract (L. extract). The combination was then filtered, and the filtrate was stored at 4 °C for further characterization.

Synthesis of *M. zapota* L. extract mediated silver nanoparticles (AgNPs)

A bio-assisted combustion synthesis was used in synthesizing the sample of AgNPs[40]. First, 1.69 g of $AgNO_3$ was calculated for the stoichiometric amount and put into a combustion crucible. Then, 5 mL of freshly extracted *M. zapota* L. extract was added as a fuel along with the double-distilled water, and the combination was allowed to agitate for 30 min to get a highly neutral solution. The same was introduced into a preheated muffle furnace maintained at a temperature of 500 °C, resulting in a typical combustion product that was taken to obtain the black amorphous product. Additionally, the obtained sample was calcined for 2 h at 750 °C to obtain AgNPs of the desired phase. A brief synopsis of the synthesis process is depicted in Fig. 1. The same was conducted in triplicate to achieve the appropriate yield 1.086 g, 64.3%) sufficient for sample characterization.

Catalyst activity against MB dye

The bio-combusted AgNPs were utilized as a photocatalyst in removing 10 ppm (10 mg/L) MB dye solution in acidic medium, conducted in a 3 mL cuvette cell at an ambient temperature of 27 ± 5 °C. A dosage of 60 mg of the previously mentioned photocatalyst was used in these solutions. These solutions were further stirred in the dark for 60 min inside a UV chamber equipped with an amiciVision UV flashlight, attaining adsorption-desorption equilibrium. Furthermore, every 3 mL solution at a time interval (10 min) starting from the blank solution was picked and analyzed for absorption spectrum between 525 and 725 nm wavelength using Lab India's UV-3200 spectrophotometer. The degradation rate was evaluated using Eq. (1)[32],

$$\%D = \frac{A_0 - A_t}{A_0} \times 100 \tag{1}$$

Where A_0 and A_t resemble absorption at the 0th minute and particular time illumination, respectively.

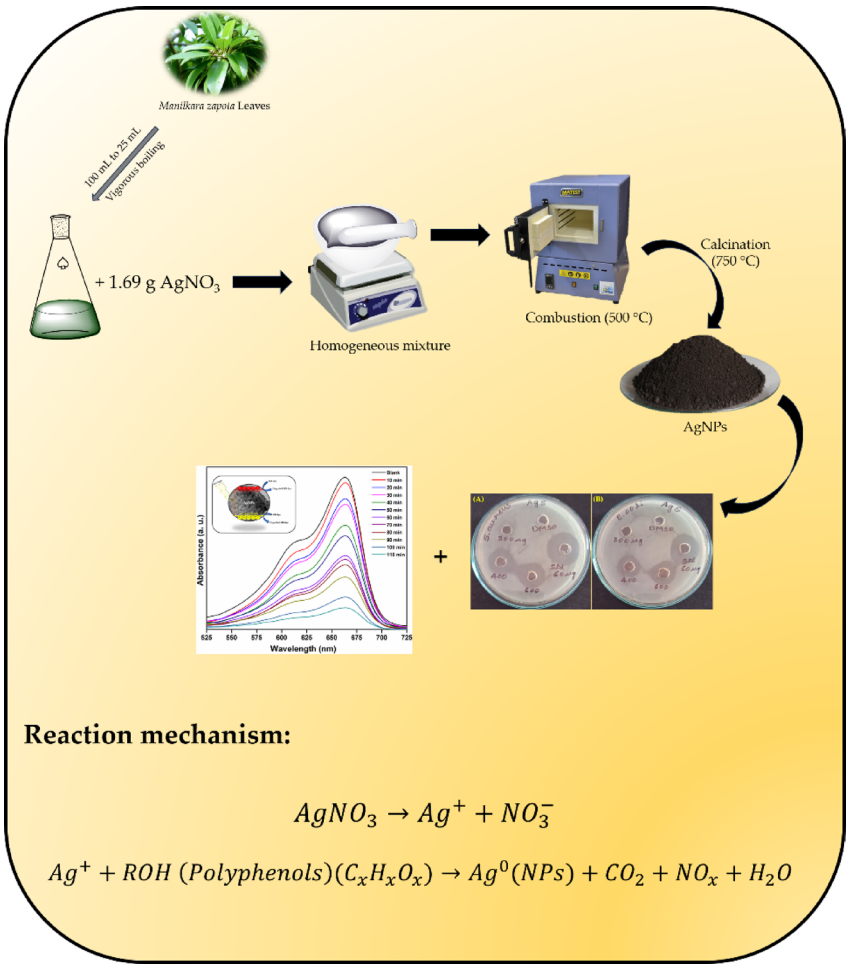

Fig. 1. Schematic representation of bio-combustion of AgNPs and its reaction mechanism involved.

Results and discussion

Absorption studies

Estimation of the band gap is important in understanding the electronic characteristics of a material, which in turn defines the appropriateness of the material for semiconductor, photocatalyst, and optical applications. Hence, a reflectance spectrum (Fig. 2a) between 200 and 600 nm was recorded for the synthesized AgNPs, which was further involved in calculating the energy band-gap using the Kubelka-Munk (K-M) relation (2)[33],

$$[F(R)] = {}^{K}/_{S} \tag{2}$$

$$K = (1-R)^2 \qquad S = 2R$$

Where R indicates the reflectance coefficient. The evaluated band-gap energy was found to be 3.31 eV as depicted in Fig. 2b.

Structural phase analysis

Powder X-ray diffraction (PXRD) analysis is of great importance in defining the phases and structural details of nanomaterials, which act as a key factor in a wide range of applied fields. The prepared AgNPs were characterized by a powder X-ray diffraction (PXRD) technique to provide structural information. Figure 3 depicts the diffracted peaks of AgNPs in accordance with JCPDS card #96-901-3046, thus confirming that the observed phase is cubic (Fm-3 m). The obtained parameters were ($\alpha = \beta = \gamma = 90°$ and $a = b = c = 4.0860$ Å). Planes (111), (200), (220), (311), and (222) were allocated to $2\theta = 38.14°$, 44.32°, 64.46°, 77.43°, and 81.56°, respectively. For the same peak values, Scherrer's relation (3) was applied in evaluating the average crystallite size[34].

$$D_{hkl} = \frac{0.9 * \lambda}{\beta_{hkl} \cos\theta} \tag{3}$$

Where, D_{hkl} is referred to as crystallite size, β_{hkl} as Half Maximum of Full Width (FWHM) of the observed peaks. Also, θ resembles the diffracting angle, and λ is the wavelength of the X-rays used. The average crystallite size was evaluated to be 22.38 nm. The same was affirmed by applying the Williamson-Hall (W-H) relation (4) for the obtained results, as shown in Fig. 4[35]. The obtained value was well aligned with the crystallite size from the PXRD analysis (24.75 nm) with a strain component (ε) value of 3.2×10^{-3} and R^2 value of 0.987.

$$\beta_{hkl} \cos\theta = 4\epsilon \sin\theta + \frac{0.9\lambda}{D_{hkl}} \tag{4}$$

The same was verified by the Stress-Strain Plot (SSP) (Text S1), which was found to be Dhkl = 25.02 nm and $\varepsilon = 5.4 \times 10^{-3}$ (Figure S1).

IR studies

The vital part of molecular analysis using vibrational transitions is in determining molecular structures and the chemical composition of a particular object. Figure 5 demonstrates the IR spectra recorded between 500 and 4000 cm^{-1} of both *M. zapota* L. extract and AgNPs. Prominent bands at 849 cm^{-1}, 882 cm^{-1}, 1105 cm^{-1}, 1444 cm^{-1}, 1554 cm^{-1}, 1656 cm^{-1}, and 3335 cm^{-1} were observed. Upon referring to the available literature, the band at 3335 cm^{-1} is assigned to O-H stretching. Bands at 1105, 1444/1554, and 1656 cm^{-1} can be attributed to C-N stretching, N-H stretching, and C = C/C = O moieties, respectively. The band ranging between

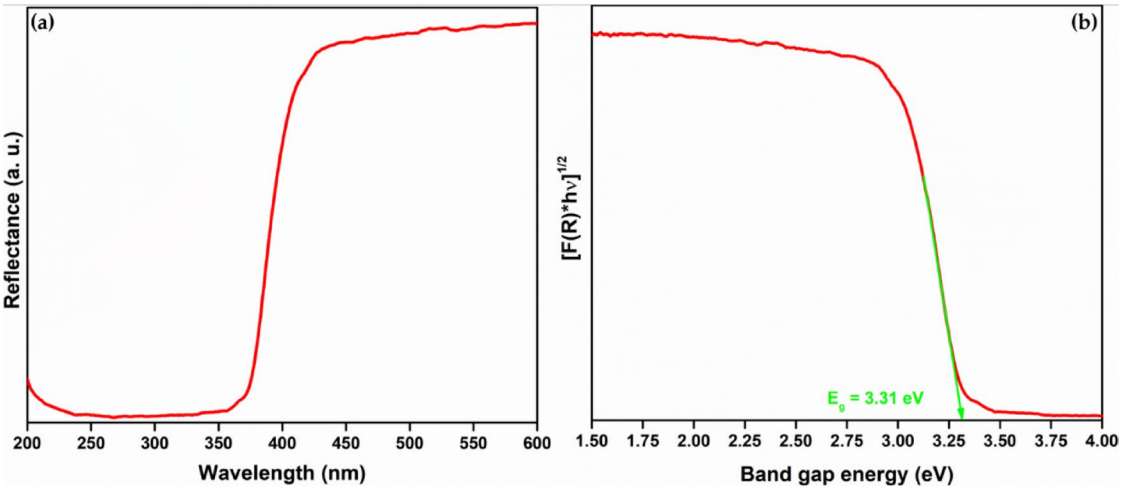

Fig. 2. (**a**) Recorded reflectance spectrum and (**b**) K-M plot of synthesized AgNPs.

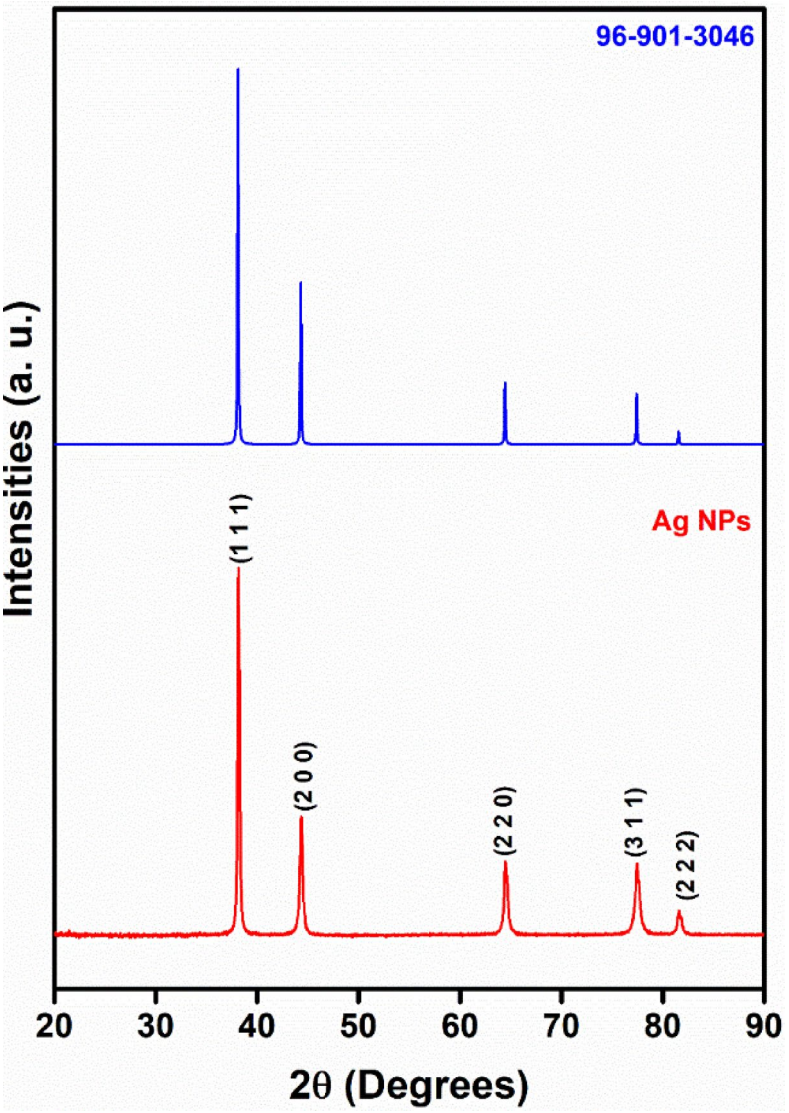

Fig. 3. PXRD profile of as-prepared AgNPs is in good agreement with the card #96-901-3046.

2458–1897 cm^{-1} is attributed to C-H stretching from methylene groups. At last, the bands at 849 cm^{-1} and 882 cm^{-1} were observed due to the presence of metal peroxides (Ag-O) (< 1000 cm^{-1})[36–39].

Morphology

Morphology evaluation is one of the key aspects in predicting the functional properties of nanostructures since it is associated with material shape and size distribution. Hence, the as-synthesized AgNPs were subjected to study the shape and size distribution using SEM and TEM microscopy. Figure 6 depicts the SEM images at 3 µm (Fig. 6A), 2 µm (Fig. 6B), 1 µm (Fig. 6C), and a magnified version of Fig. 6B (Fig. 6D), showing an agglomerated assembly morphology for synthesized AgNPs. This agglomeration may be due to the usage of green fuel and calcinating temperature after combustion synthesis[40]. Figure 7 presents the EDX spectrum, which confirms the elemental composition of the synthesized AgNPs. The peaks indicating the major components are silver (Ag), exhibiting a notably high weight% of approximately 76.5%. The presence of oxygen (~ 17.5%) suggests the potential existence of surface oxide or phytochemical capping derived from the extract of *M. zapota* L. A minor carbon signal (~ 5.9%) is apparent, likely resulting from residual plant metabolites or adsorbed atmospheric CO_2 during the sample preparation process. The results validate the effective green synthesis of AgNPs with high purity, and the elemental composition aligns with the PXRD and FTIR analyses, further substantiating both the structure and composition of the nanomaterial.

Figure 8 (a–c) shows the TEM images of as-synthesized AgNPs at 500, 100, and 50 nm magnification, confirming the agglomeration of AgNPs in the clusters. The same has been utilized in evaluating the average particle size of ~ 24 nm using the line tool in ImageJ software (ImageJ 1.53t, https://imagej.net/ij/). This result is aligned with the calculated crystallite size in PXRD analysis. Also, Fig. 8d indicates the two prominent peaks (111) and (200) and confirms the crystallinity of the sample. At last, Fig. 8e and f show the HRTEM resolution of

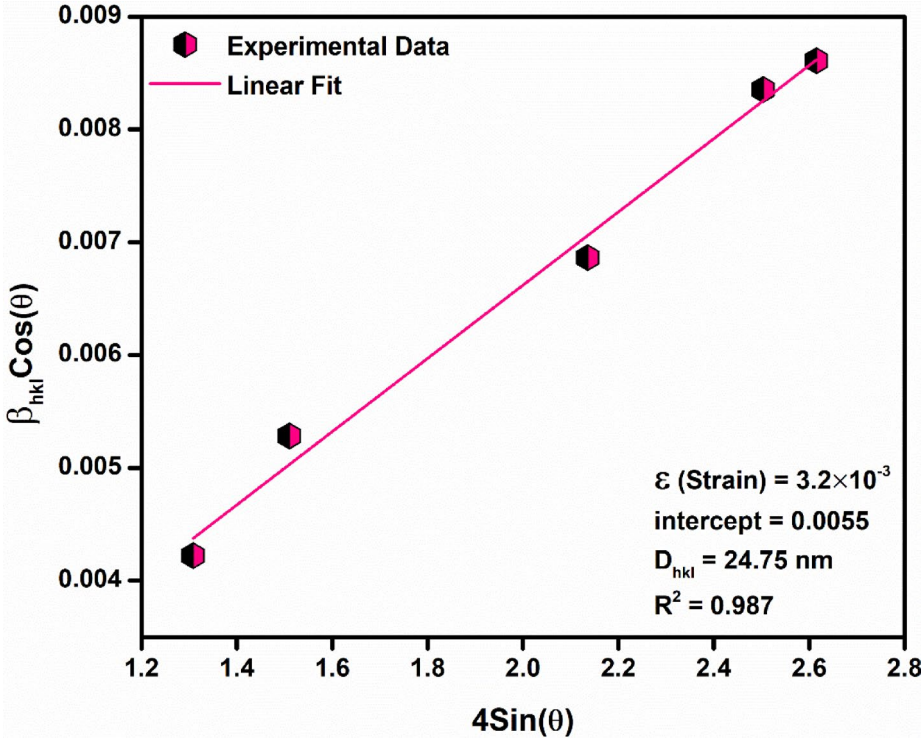

Fig. 4. W-H plot of AgNPs using the respective diffraction peaks.

the sample, which is used further to evaluate the d-spacing value, which is to be found at 0.351 nm. Further, the same TEM images have been utilized to obtain the particle size distribution histogram as shown in Fig. 8g, which is well aligned with the evaluated average particle size of ~ 24 nm, which was further authenticated by particle size analysis of the recorded DLS data as depicted in Figure S2 of the supporting information.

Catalytic activity of as-synthesized AgNPs against MB dye

The removal of cationic MB dye was observed through absorption studies conducted using a UV-visible spectrophotometer between 525 and 725 nm wavelengths, as seen in Fig. 9(a). Initially, a UV chamber equipped with an AmiciVision UV flashlight was utilized to conduct the absorbance studies. 60 mg of AgNPs catalyst was added to 100 mL MB dye solution with a 10 ppm concentration and stirred in the dark for 60 min to attain the adsorption-desorption equilibrium. Later, once the illumination was made, 3 mL solution was taken out every 10 min for recording the absorption spectrum. The dye observed a noticeable 83.33% degradation after 110 min of UV illumination inside a UV chamber (Fig. 9b). Further, the same absorbance results were utilized in studying the degradation using the zeroth-order kinetic relation (5)[41],

$$A_t = A_0 - kt \tag{5}$$

This shows that the degradation results were best aligned with $R^2 = 0.98$ and $k_0 = 0.007$ as depicted in Fig. 9c.

Investigating the pH influence on dye degradation is vital as the pH affects both the efficacy and mechanism of degradation, thus affecting the general effectiveness of existing treatment procedures in removing dyes from water. Hence, the solution containing 10 ppm of MB dye and 60 mg of prepared catalyst, AgNPs, was maintained at pH levels 2, 4, 6, and 8 using a suitable buffer. The same was kept under UV illumination to examine the degradation of MB dye, and found that the maximum dye removal occurred in acidic medium (pH 2) (Fig. 9d).

Furthermore, the degradation rates were also studied in the presence of different scavengers. The selected scavengers: (i) Ascorbic Acid (AA), (ii) Ethylenediamine tetraacetic acid (EDTA), and (iii) 2 Propanol (IPA) serve as the trappers of superoxide radicals ($\cdot O_2^-$), holes (h^+), and hydroxyl radicals ($\cdot OH$), which are responsible for dye removal. Results depicted in Fig. 10 reveal that the MB degradation was minimally affected by the selected scavengers. AA affects the degradation rate from 83.3% to 79.5%, EDTA, to 79.8%, and IPA, to 80.8%.

Degradation mechanism

When UV-Vis light is exposed to a photocatalyst, an electron (e) is excited from the valence band into the conduction band, generating a positive hole (h^+). The cleavage of water molecules by h^+ or e^- reduces surface absorbed oxygen species to produce superoxide ions (0^{2-})[42–44]. Nevertheless, in either case, highly reactive hydroxyl radicals attack certain organic compounds, thus permitting their decomposition into smaller intermediates and finally carbon dioxide (CO_2) and water (H_2O) without any danger[45–49]. All the observed results and the scavenger effect suggest a possible degradation mechanism proposed in Fig. 11.

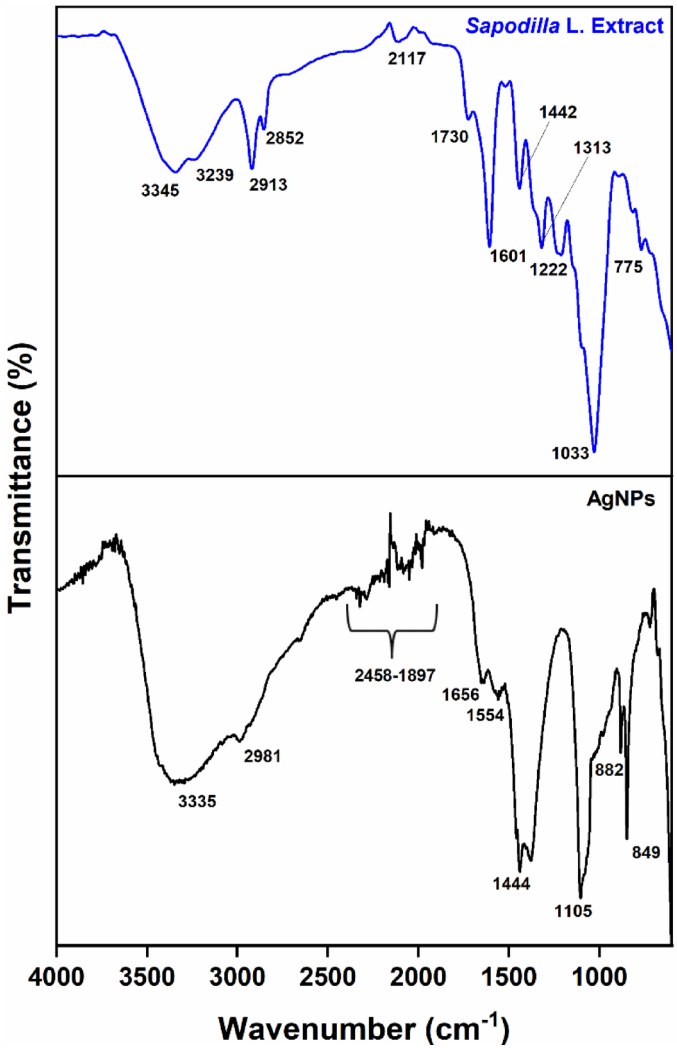

Fig. 5. Recorded FT-IR spectrum of as-synthesized AgNPs.

Antibacterial activity

The as-synthesized AgNPs were evaluated for antimicrobial activity by agar well diffusion method, as described by previous reports[50], with slight modifications. The prepared AgNPs were labeled as AgS for convenience purposes and tested against the bacterial strains, gram-positive *Staphylococcus aureus* MTCC-7443 and gram-negative *Escherichia coli* MTCC-7410. The inoculum was adjusted to approximately 5×10^5 CFU/mL with sterile saline solution. The sample was dissolved at 10 mg/mL in DMSO as a stock solution and loaded into different concentration ranges, 200 µg to 600 µg, for different wells. The medium used was Muller Hinton agar (Hi-media) and incubation at 37 °C for 12 h After incubation, the diameter of the inhibition zone (mm) was measured. The results tabulated in Table 1 show that the prepared sample was active for both gram-positive and gram-negative beyond 400 µg/mL, which is shown in Fig. 12 in comparison with standard drugs, Penicillin G for gram-positive and Ciprofloxacin for gram-negative bacterial species at 60 µg/mL.

The synthesized AgNPs have shown strong antibacterial action against both Gram-positive *Staphylococcus aureus* and Gram-negative *Escherichia coli* pathogens, with greater inhibition at doses over 400 µg/mL. Greater inhibition zone widths with higher nanoparticle concentrations indicate a dose-dependent impact of antibacterial activity. The somewhat increased sensitivity shown in *E. coli* compared to *S. aureus* may be explained by structural changes in the cell wall. Gram-negative bacteria have an outer membrane containing negatively charged lipopolysaccharides, which may interact electrostatically with positively charged AgNPs surfaces, increasing nanoparticle uptake. Gram-positive bacteria, on the other hand, have a thicker peptidoglycan coating that may inhibit nanoparticle penetration and hence provide a reduced sensitivity.

The mechanism for AgNPs' antibacterial effect is considered to be complex. First, AgNPs attach to the bacterial cell's surface, disrupting membrane permeability and integrity. This causes the leaking of critical intracellular components, which leads to cell lysis. AgNPs produce reactive oxygen species (ROS) such as hydroxyl radicals (•OH), superoxide anions (O_2^-), and hydrogen peroxide (H_2O_2), causing oxidative stress and damage to bacterial proteins, lipids, and nucleic acids. AgNPs produce Ag^+ ions, which attach to thiol (-SH) groups in bacterial enzymes and proteins. This inhibits respiratory enzymes and ATP synthesis. Furthermore,

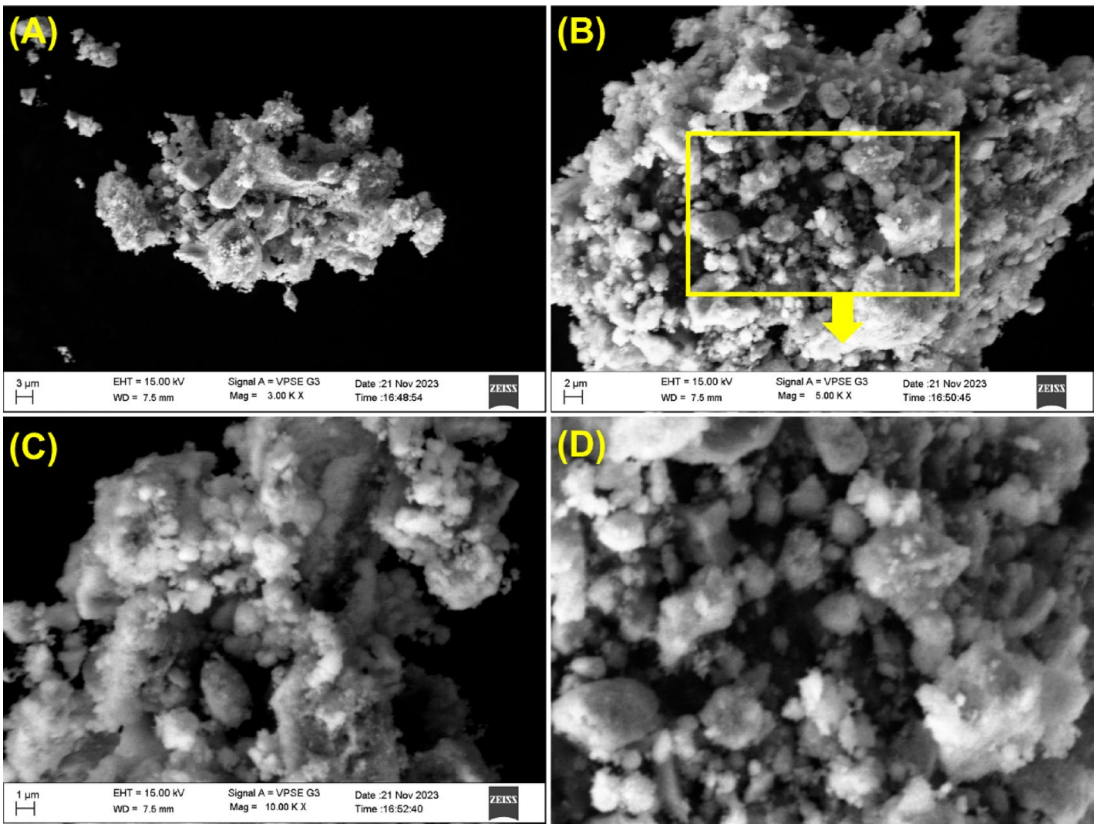

Fig. 6. SEM images at different magnifications (**A**) 3 µm, (**B**) 2 µm, (**C**) 1 µm, and (**D**) magnified region of (B) 2 µm.

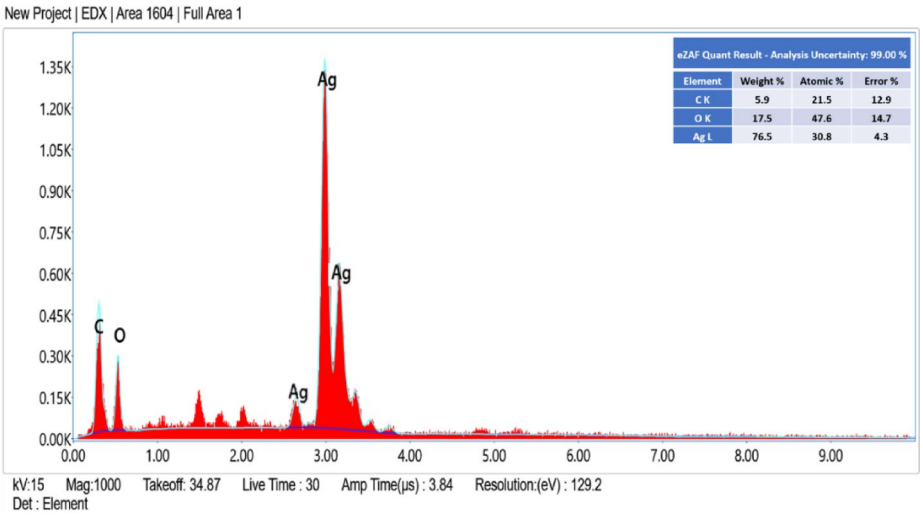

Fig. 7. EDAX spectrum of AgNPs affirming the precursor elements.

Ag^+ ions may bind to bacterial DNA and hinder replication and transcription activities. These combinatorial actions lead to the effective destruction of bacterial cells. Thus, AgNPs' antibacterial effect is the result of a combination of physical membrane rupture, chemical interaction via ion release, and oxidative stress induction. The variety of these pathways not only increases the efficacy of AgNPs but also reduces the likelihood of bacterial resistance development, making them ideal candidates for use in antimicrobial coatings, wound care products, and disinfectant applications[51,52]. Further, the comparative analysis of reported AgNPs and its photocatalytic and antibacterial activities are tabulated in Table 2.

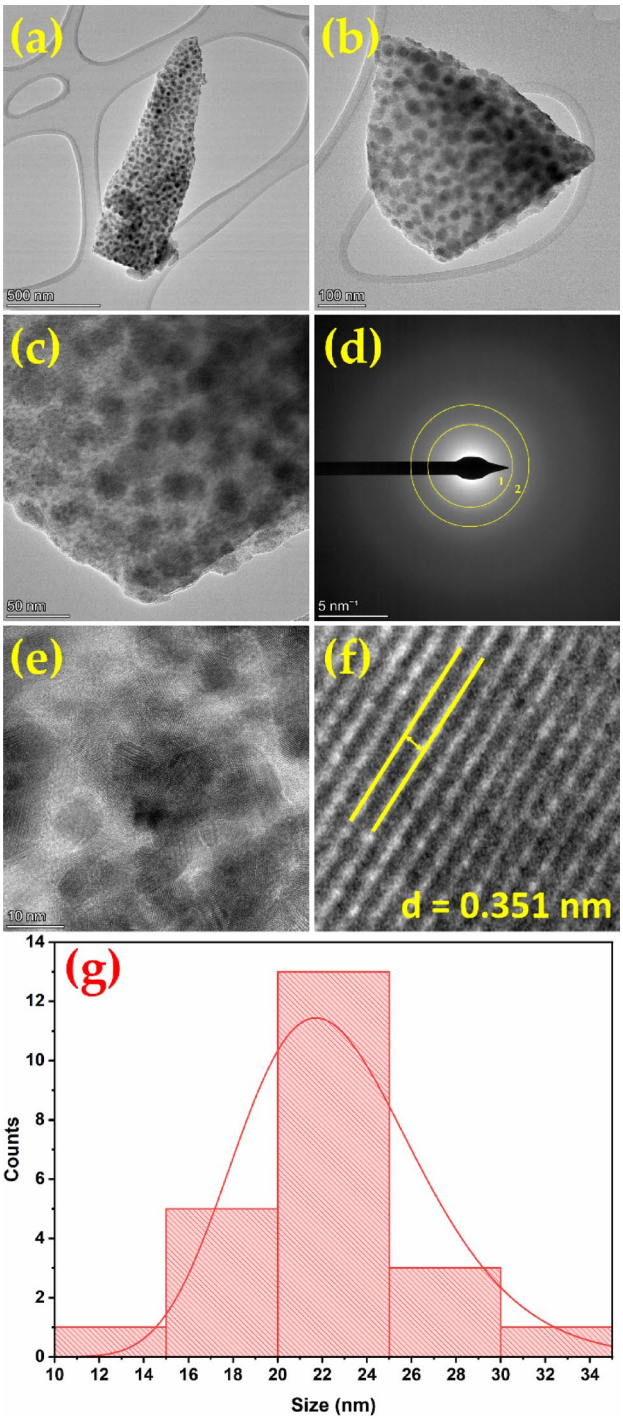

Fig. 8. (**a–c**) TEM images of synthesized AgNPs at 500, 100, and 50 nm, respectively. (**d**) SAED image affirming two prominent peaks (111) and (200), (**e**, **f**) HRTEM images with d-spacing evaluation, and (**g**) obtained particle size distribution histogram.

Conclusion

To sum up, AgNPs were successfully synthesized using *M. zapota* leaf extract as a reducing agent through a simple bio-combustion method. The synthesized AgNPs were characterized for optical, phase, and morphology using various analytical techniques such as UV-Visible spectroscopy, PXRD, SEM, and TEM. The optical studies reveal that the band-gap energy of the as-synthesized AgNPs is 3.31 eV. The structural evaluation of as-prepared AgNPs aligns the observed peaks with JCPDS #96-901-3046 with a cubic phase and Fm-3 m space group. The calculated crystallite size was found to be 22.38 nm, and the same was affirmed by the W-H plot (24.75 nm). Further, the IR spectral analysis reveals the characteristic O-H stretching peak at 3335 cm^{-1} and metal-peroxide peak at 849 cm^{-1} (< 1000 cm^{-1}). The clustered agglomeration was characterized with SEM and TEM images.

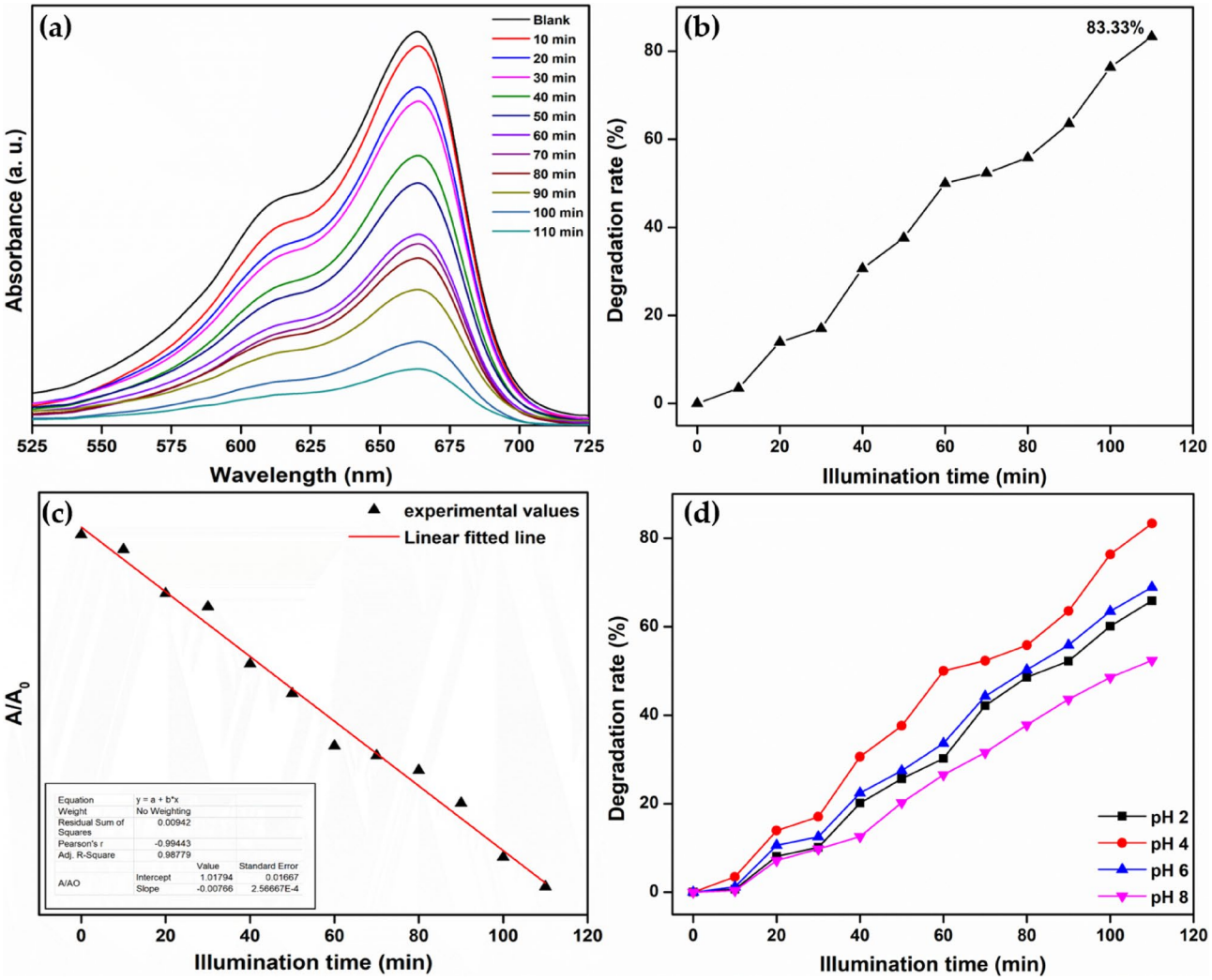

Fig. 9. (**a**) Time-sensitive absorption spectrum depicting the degradation of cationic MB dye, (**b**) time-sensitive degradation rate curve, (**c**) zeroth-order kinetics plot, and (**d**) pH effect on degradation rate of MB dye.

Initial precursors were also affirmed through EDAX analysis. Furthermore, the prepared sample was utilized in degrading the cationic dye, MB, through absorption studies. The results show a noticeable 83.33% degradation, which aligns with 0th order kinetics ($R^2 = 0.98$, $k_0 = 0.007$). pH effect reveals that the maximum degradation rate was observed in the acidic medium (pH 2). Also, a minute decrement was observed in the degradation rate after the incorporation of selected scavengers into the degradation solutions. The as-prepared AgNPs were used to evaluate the antibacterial potency against *Staphylococcus aureus* (gram-positive) and *Escherichia coli* (gram-negative) bacterial strains. The results affirm a responsive activeness from 400 µg/mL against both the bacterial strains. All the observed results suggest that the as-prepared AgNPs as a potent catalytic and antibacterial agent.

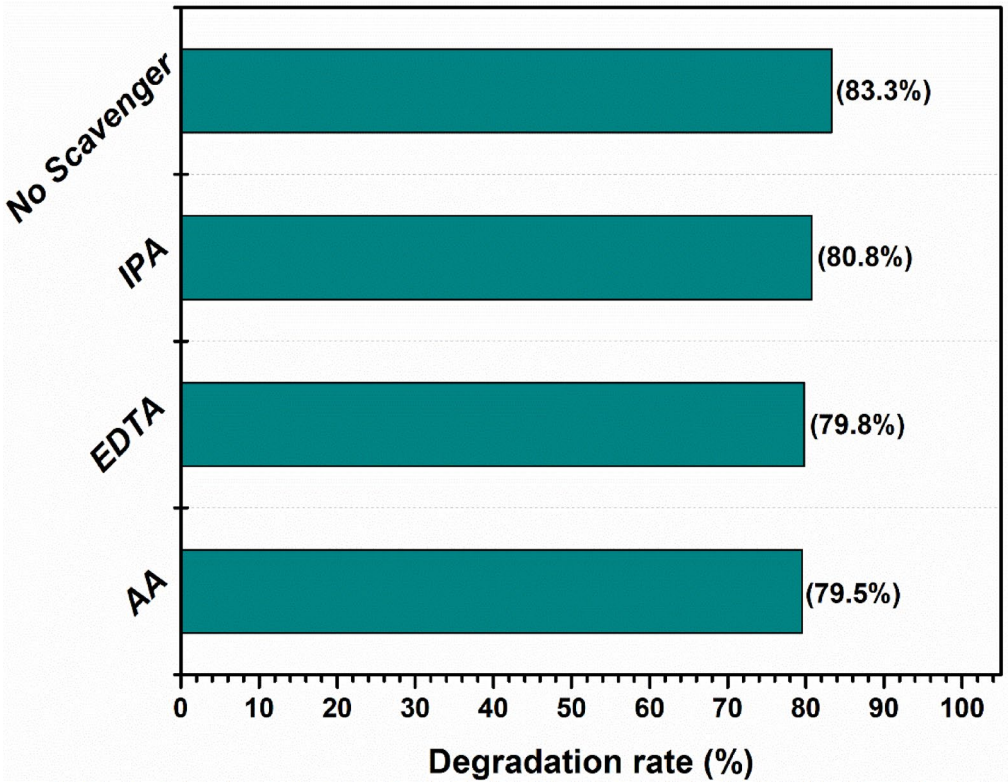

Fig. 10. Scavenger effect of as-synthesized AgNPs on the degradation rate of MB dye.

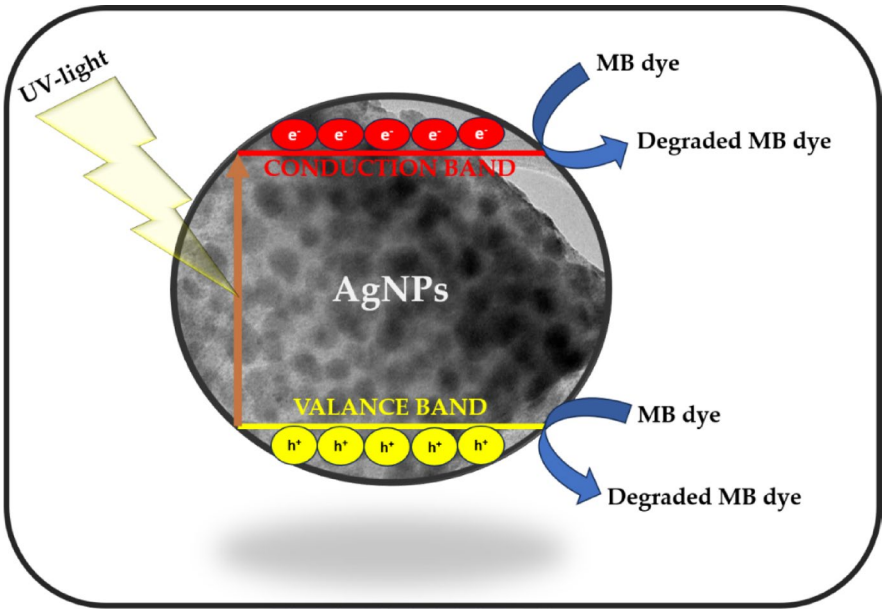

Fig. 11. Suggested photo-degradation of MB dye using AgNPs.

Sample Code	Conc. (µg/mL)	Inhibition Zone against Staphylococcus aureus (mm)	Inhibition Zone against Escherichia coli (mm)
AgS Standard drug	DMSO	–	–
	200	–	–
	400	14.66 ± 0.57	13.33 ± 1.15
	600	17.33 ± 0.57	15.33 ± 0.57
	60	19.33 ± 0.57	17.66 ± 0.57

Table 1. Antibacterial test results against two bacterial strains.

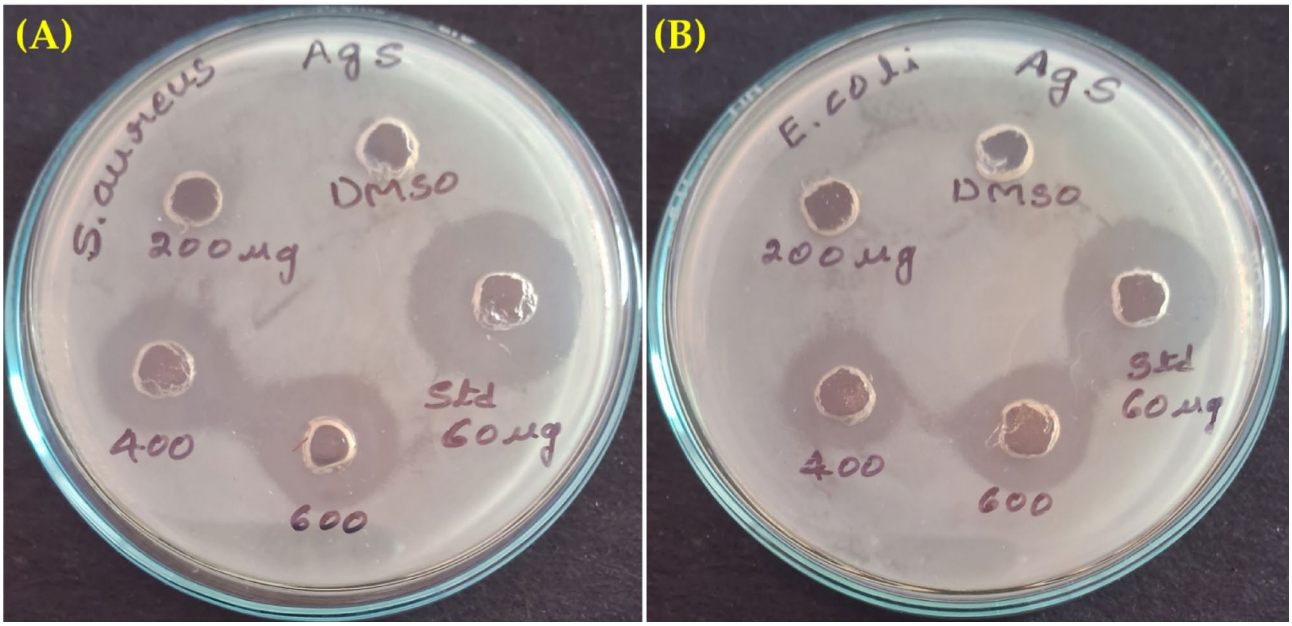

Fig. 12. Images depicting the antibacterial activity of as-synthesized AgNPs against (**A**) *S. aureus* and (**B**) *E. coli*.

Sl. No.	Green extract	Photocatalysis efficiency (Degradation%)	Antibacterial efficacy IZ (Inhibition Zone)	References
1	Kiwi fruit peel	94.2% (Congo Red)	*S. aureus* (14 mm for 50 µg/mL) and *E. coli* (16 mm for 50 µg/mL)	53
2	*Centaurea behen* leaf extract	98% (Safranin O)	*S. aureus* (11 mm for 240 µg/mL), *S. epidermidis* (10 mm for 240 µg/mL), *M. luteus* (15 mm for 240 µg/mL) and *E. coli* (10 mm for 240 µg/mL)	54
3	*Pandanus tectorius* root extract	82.6% (Methylene Blue)	*P. aeruginosa* (13 mm for 100 µg/mL)	55
4	*Cassia fistula* flower extract	83.82% (Methylene Blue) and 65.14% (Crystal Voilet)	*S. aureus* (16.2 mm for 250 µg/mL) and *E. coli* (11.8 mm for 50 µg/mL)	56
5	*Santalum album* L. extract	71.3% (Malachite Green) and 92.14% (Methylene Blue)	*S. aureus* (17.2 mm for 500 µg/mL) and *P. aeruginosa* (12.3 mm for 500 µg/mL)	57

Table 2. Comparison analysis of various AgNPs as potential catalytic and antibacterial agents.

Data availability

All the data generated or analyzed during this study are included within the article and supporting information file.

Received: 14 May 2025; Accepted: 8 December 2025
Published online: 11 December 2025

References

1. Silva-Holguín, P. N., Garibay-Alvarado, J. A. & Reyes-López, S. Y. Silver Nanoparticles: Multifunctional Tool in Environmental Water Remediation. *Materials, 17(9)*, 1939. https://www.mdpi.com/1996-1944/17/9/1939 (2024).
2. Zha, S. et al. Functionalized nanomaterials capable of crossing the Blood–Brain barrier. *ACS Nano*. **18** (3), 1820–1845. https://doi.org/10.1021/acsnano.3c10674 (2024).

3. Sher, F. et al. Magnetic multifunctional nanomaterials for enhanced transverse chemical and bioanalytical applications – A review. *TRAC Trends Anal. Chem.* **173**, 117622. https://doi.org/10.1016/j.trac.2024.117622 (2024).
4. Song, K. et al. Functional inorganic nanomaterials for optical cancer theranostics. *Chem. Eng. J.* **485**, 150067. https://doi.org/10.1016/j.cej.2024.150067 (2024).
5. M, A. M., Ashwin, D. U., Yardily, B. M., Dennison, M. S. & A., & Microwave-assisted green synthesized ZnO nanoparticles: an experimental and computational investigation. *Discover Appl. Sci.* **7** (3), 177. https://doi.org/10.1007/s42452-025-06563-8 (2025).
6. Lithi, I. J., Nakib, A., Chowdhury, K. I., Sahadat Hossain, M. & A. M. S., & A review on the green synthesis of metal (Ag, Cu, and Au) and metal oxide (ZnO, MgO, Co3O4, and TiO2) nanoparticles using plant extracts for developing antimicrobial properties. *Nanoscale Adv.* **7** (9), 2446–2473. https://doi.org/10.1039/D5NA00037H (2025).
7. Natarajan, A. et al. Silver nanoparticles based functional materials for Anti-bacterial and antiviral applications. *Antibact. Antiviral Funct. Mater.* **2**, 185–219. https://doi.org/10.1021/bk-2024-1472.ch006 (2024).
8. Ardra Lekshmi, A. et al. Green synthesis of silver nanoparticles: A one-pot approach with emphasis on antibacterial, antifungal, and biosensor applications. *Mater. Today: Proc.* **(In Press)** https://doi.org/10.1016/j.matpr.2024.05.121 (2024).
9. El-Sofany, W. I., Azzam, E. M. S., Latif, S. & Hamden, K. Spirothiazolidine-Derivative on Silver Nanoparticles and Carbon Nanotubes: Evaluation of Antibacterial, Anti-Fungal, Anti-Inflammatory,Antioxidant and Gastroprotective Activities. *Pharmaceutics*, *16*(7), 901. https://www.mdpi.com/1999-4923/16/7/901 (2024).
10. Sharifi-Rad, M., Elshafie, H. S. & Pohl, P. Green synthesis of silver nanoparticles (AgNPs) by lallemantia Royleana leaf extract: their Bio-Pharmaceutical and catalytic properties. *J. Photochem. Photobiol., A.* **448**, 115318. https://doi.org/10.1016/j.jphotochem.2023.115318 (2024).
11. Said, A., Abu-Elghait, M., Atta, H. M. & Salem, S. S. Antibacterial activity of green synthesized silver nanoparticles using lawsonia inermis against common pathogens from urinary tract infection. *Appl. Biochem. Biotechnol.* **196** (1), 85–98. https://doi.org/10.1007/s12010-023-04482-1 (2024).
12. Singh, S. et al. Green synthesized silver nanoparticles of terminalia Bellirica leaves extract: synthesis, characterization, in-silico studies, and antimalarial activity. *Artif. Cells Nanomed. Biotechnol.* **52** (1), 238–249. https://doi.org/10.1080/21691401.2024.2339429 (2024).
13. Gam, S. et al. A systematic review on traditional use, phytochemistry and Pharmacological activities of *Manilkara Zapota*. *Pharmacol. Res. - Nat. Prod.* **4**, 100062. https://doi.org/10.1016/j.prenap.2024.100062 (2024).
14. Burelo, M. et al. Recent Developments in Synthesis, Properties, Applications and Recycling of Bio-Based Elastomers. *Molecules*, *29*(2), 387. https://www.mdpi.com/1420-3049/29/2/387 (2024).
15. Sahu, K., Kurrey, R. & Pillai, A. K. Green synthesis of silver nanoparticles from *Manilkara Zapota* leaf extract for the detection of aminoglycoside antibiotics and other applications [10.1039/D4RA01906G]. *RSC Adv.* **14** (32), 23240–23256. https://doi.org/10.1039/D4RA01906G (2024).
16. Yong, K. Y. & Abdul Shukkoor, M. S. *Manilkara Zapota*: A phytochemical and pharmacological review. *Materials Today: Proceedings*, *29*, 30–33. https://doi.org/10.1016/j.matpr.2020.05.688 (2020).
17. Punia Bangar, S. et al. A review of Sapodilla (*Manilkara zapota*) in human nutrition, health, and industrial applications. *Trends Food Sci. Technol.* **127**, 319–334. https://doi.org/10.1016/j.tifs.2022.05.016 (2022).
18. Shahraki, S. H., Javar, F. M. & Rahimi, M. Quantitative and qualitative phytochemical analysis of *Manilkara Zapota* (Sapodilla) extract and its antibacterial activity on some Gram-Positive and Gram-Negative bacteria. *Scientifica* **2023** (1), 5967638. https://doi.org/10.1155/2023/5967638 (2023).
19. Olas, B., Urbańska, K. & Bryś, M. Saponins as modulators of the blood coagulation system and perspectives regarding their use in the prevention of venous thromboembolic incidents. *Molecules* **25** (21), 5171. https://www.mdpi.com/1420-3049/25/21/5171 (2020).
20. de Carvalho, A. T. et al. Ethnopharmacology of fruit plants: A literature review on the Toxicological, Phytochemical, cultural Aspects, and a mechanistic approach to the Pharmacological effects of four widely used species. *Molecules* **25** (17), 3879. https://www.mdpi.com/1420-3049/25/17/3879 (2020).
21. Karam, S. T. & Abdulrahman, A. F. Green synthesis and characterization of ZnO nanoparticles by using thyme plant leaf extract. *Photonics* **9** (8), 594. https://www.mdpi.com/2304-6732/9/8/594 (2022).
22. Swamy, M. M. et al. Eco-friendly development of leucas aspera-derived MoO3 nanoparticles: corrosion studies and multifunctional applications in medicine, agriculture, and industry. *Appl. Phys. A.* **131** (1), 71. https://doi.org/10.1007/s00339-024-08199-8 (2025).
23. Surendra, B. S. et al. Emerging applications of sustainable modified CdO/Ag-CdO NPs for electrochemical sensitive and selective detection of mercury (Hg+) heavy metal. *Sci. Rep.* **15** (1), 28200. https://doi.org/10.1038/s41598-025-11691-7 (2025).
24. Abdullah, J. A. A., Jiménez-Rosado, M., Guerrero, A. & Romero, A. Effect of calcination temperature and time on the synthesis of iron oxide nanoparticles: green vs. *Chem. Method Materials*. **16** (5), 1798. https://www.mdpi.com/1996-1944/16/5/1798 (2023).
25. Elwakil, B. H., Eldrieny, A. M., Almotairy, A. R. Z. & El-Khatib, M. Potent biological activity of newly fabricated silver nanoparticles coated by a carbon shell synthesized by electrical Arc. *Sci. Rep.* **14** (1), 5324. https://doi.org/10.1038/s41598-024-54648-y (2024).
26. Miškovská, A. et al. Biological activity of silver nanoparticles synthesized using viticultural waste. *Microb. Pathog.* **190**, 106613. https://doi.org/10.1016/j.micpath.2024.106613 (2024).
27. Ohiduzzaman, M. et al. Crystallographic structure, antibacterial effect, and catalytic activities of Fig extract mediated silver nanoparticles. *Heliyon* **10** (11), e32419. https://doi.org/10.1016/j.heliyon.2024.e32419 (2024).
28. Ahmed, B., Bilal Tahir, M., Sagir, M. & Hassan, M. Bio-inspired sustainable synthesis of silver nanoparticles as next generation of nanoproduct in antimicrobial and catalytic applications. *Mater. Sci. Engineering: B*. **301**, 117165. https://doi.org/10.1016/j.mseb.2023.117165 (2024).
29. Tze-Wei, B. T. et al. (eds) b., Properties of Natural Rubber: Magnetite Decorated with Silver Nanoparticles for Catalytic Degradation of Model Organic Contaminant. *Journal of Inorganic and Organometallic Polymers and Materials*. https://doi.org/10.1007/s10904-023-02933-0 (2024).
30. Hamat, A. B. A. C. et al. V., P. Cocos Nucifera's lignin mediated silver nanoparticle and their photocatalytic activity. *Inorganic Chemistry Communications*, *160*, 111845. https://doi.org/10.1016/j.inoche.2023.111845 (2024).
31. Varadavenkatesan, T., Nagendran, V., Vinayagam, R., Goveas, L. C. & Selvaraj, R. Effective degradation of dyes using silver nanoparticles synthesized from thunbergia grandiflora leaf extract. *Bioresource Technol. Rep.* **27**, 101914. https://doi.org/10.1016/j.biteb.2024.101914 (2024).
32. Majani, S. S., Basavaraj, R. B., Iqbal, M., Venkatachalaiah, K. N. & Kollur, S. P. Dysprosium doped SrCeO3 nanophosphors for advanced photochemical applications: Synthesis, characterization, photo-assisted dye degradation and latent fingerprint visualization. *Mater. Sci. Semiconduct. Process.* **182**, 108674. https://doi.org/10.1016/j.mssp.2024.108674 (2024).
33. Ait-karra, A. et al. Effect of hydrothermal temperature on the structural, morphological, optical properties and photocatalytic performances of Cobalt sulfide nanomaterials. *J. Alloys Compd.* **999**, 174946. https://doi.org/10.1016/j.jallcom.2024.174946 (2024).
34. Sukarman, Kristiawan, B., Khoirudin, Abdulah, A., Enoki, K. & Wijayanta, A. T. Characterization of TiO2 nanoparticles for nanomaterial applications: crystallite size, microstrain and phase analysis using multiple techniques. *Nano-Structures Nano-Objects*. **38**, 101168. https://doi.org/10.1016/j.nanoso.2024.101168 (2024).
35. Disha, S. A., Sahadat Hossain, M., Habib, M. L. & Ahmed, S. Calculation of crystallite sizes of pure and metals doped hydroxyapatite engaging scherrer method, Halder-Wagner method, Williamson-Hall model, and size-strain plot. *Results Mater.* **21**, 100496. https://doi.org/10.1016/j.rinma.2023.100496 (2024).

36. Gamal, W. M., El-Bassuony, A. A. H. & Abdelsalam, H. K. Fascinating study of elastic, FTIR, and antimicrobial properties of silver nanochromite at different annealing temperatures. *Polym. Bull.* **81** (2), 1821–1837. https://doi.org/10.1007/s00289-023-04788-4 (2024).
37. Al-Sahli, S. A., Al-Otibi, F., Alharbi, R. I., Amina, M. & Al Musayeib, N. M. Silver nanoparticles improve the fungicidal properties of rhazya stricta decne aqueous extract against plant pathogens. *Sci. Rep.* **14** (1), 1297. https://doi.org/10.1038/s41598-024-51855-5 (2024).
38. Tunç, T., Hepokur, C. & Karîper, A. Synthesis and characterization of Paclitaxel-Loaded silver nanoparticles: evaluation of cytotoxic effects and antimicrobial activity. *Bioinorg. Chem. Appl.* **2024** (1), 9916187. https://doi.org/10.1155/2024/9916187 (2024).
39. Vinayagam, R. et al. Structural characterization of marine macroalgae derived silver nanoparticles and their colorimetric sensing of hydrogen peroxide. *Mater. Chem. Phys.* **313**, 128787. https://doi.org/10.1016/j.matchemphys.2023.128787 (2024).
40. Majani, S. S., Manoj, Lavanya, Swathi, B., Anuvarna, N., Iqbal, M. & Kollur, S. P. Nano-catalytic behavior of CeO_2 nanoparticles in dye adsorption: synthesis through Bio-combustion and assessment of UV-light-driven Photo-adsorption of Indigo Carmine dye. *Heliyon* **10**, e35505. https://doi.org/10.1016/j.heliyon.2024.e35505 (2024).
41. Razali, N. A. & Othman, S. A. Kinetic study of photocatalytic degradation of reactive black 5. *AIP Conf. Proc.* **2347** (1). https://doi.org/10.1063/5.0051495 (2021).
42. Karthikeyan, S., Dhanakodi, K., Shanmugasundaram, K. & Surendhiran, S. Synthesis and characterization of lanthanum oxide nanoparticles: A study on the effects of surfactants. *Materials Today: Proceedings*, 47, 901–906. https://doi.org/10.1016/j.matpr.2021.04.473 (2021).
43. Yadav, A. A., Lokhande, A. C., Pujari, R. B., Kim, J. H. & Lokhande, C. D. The synthesis of multifunctional porous honey comb-like La2O3 thin film for supercapacitor and gas sensor applications. *J. Colloid Interface Sci.* **484**, 51–59. https://doi.org/10.1016/j.jcis.2016.08.056 (2016).
44. Liu, Y. et al. Efficient blue light-emitting diodes based on quantum-confined bromide perovskite nanostructures. *Nat. Photonics.* **13** (11), 760–764. https://doi.org/10.1038/s41566-019-0505-4 (2019).
45. Kalia, R. et al. Photocatalytic degradation properties of Li-Cr ions substituted CoFe2O4 nanoparticles for wastewater treatment application. *Phys. Status Solidi (a).* **219** (8), 2100539. https://doi.org/10.1002/pssa.202100539 (2022).
46. Dumrongrojthanath, P., Thongtem, T., Phuruangrat, A. & Thongtem, S. Synthesis and characterization of hierarchical multilayered flower-like assemblies of ag doped Bi2WO6 and their photocatalytic activities. *Superlattices Microstruct.* **64**, 196–203. https://doi.org/10.1016/j.spmi.2013.09.028 (2013).
47. Phuruangrat, A. et al. Effect of pH on visible-light-driven Bi2WO6 nanostructured catalyst synthesized by hydrothermal method. *Superlattices Microstruct.* **78**, 106–115. https://doi.org/10.1016/j.spmi.2014.11.038 (2015).
48. Yayapao, O., Thongtem, T., Phuruangrat, A. & Thongtem, S. Ultrasonic-assisted synthesis of Nd-doped ZnO for photocatalysis. *Mater. Lett.* **90**, 83–86. https://doi.org/10.1016/j.matlet.2012.09.027 (2013).
49. Yayapao, O., Thongtem, T., Phuruangrat, A. & Thongtem, S. Sonochemical synthesis of Dy-doped ZnO nanostructures and their photocatalytic properties. *J. Alloys Compd.* **576**, 72–79. https://doi.org/10.1016/j.jallcom.2013.04.133 (2013).
50. Erhonyota, C., Edo, G. I. & Onoharigho, F. O. Comparison of poison plate and agar well diffusion method determining the antifungal activity of protein fractions. *Acta Ecol. Sin.* **43** (4), 684–689. https://doi.org/10.1016/j.chnaes.2022.08.006 (2023).
51. Atz-Dick, T., Valente, R. C., Machado, T. V., Horn, F. & Dick, L. F. P. Solid-State precipitation of silver nanoparticles nucleated during al anodizing: mechanism and antibacterial properties. *ACS Appl. Bio Mater.* **8** (2), 1466–1474. https://doi.org/10.1021/acsabm.4c01694 (2025).
52. Isah, M., Malek, N. A. N. N., Susanto, H., Asraf, M. H. & Aliero, A. S. Preparation, characterization, and antibacterial activity of Moringa oleifera–silver nanoparticles-kaolinite nanocomposite. *Appl. Clay Sci.* **269**, 107761. https://doi.org/10.1016/j.clay.2025.107761 (2025).
53. Bharathi, D. et al. Kiwi fruit Peel Biowaste mediated green synthesis of silver nanoparticles for enhanced dye degradation and antibacterial activity. *Waste Biomass Valoriz.* **15** (3), 1859–1868. https://doi.org/10.1007/s12649-023-02328-9 (2024).
54. Abdoli, M. et al. Centaurea Behen leaf extract mediated green synthesized silver nanoparticles as antibacterial and removing agent of environmental pollutants with blood compatible and hemostatic effects. *Sci. Rep.* **14** (1), 13941. https://doi.org/10.1038/s41598-024-64468-9 (2024).
55. Balamurugan, V., Ragavendran, C., Arulbalachandran, D., Fahad Alrefaei, A. & Rajendran, R. Green synthesis of silver nanoparticles using pandanus tectorius aerial root extract: Characterization, antibacterial, cytotoxic, and photocatalytic properties, and ecotoxicological assessment. *Inorg. Chem. Commun.* **168**, 112882. https://doi.org/10.1016/j.inoche.2024.112882 (2024).
56. Omran, A. M. E. Green route synthesis of silver nanoparticles driven by Cassia fistula flower extract: characterization, antioxidant, antibacterial, anticancer, and photocatalytic assessment. *Biomass Convers. Biorefinery.* **14** (17), 20405–20418. https://doi.org/10.1007/s13399-023-04520-2 (2024).
57. Selvam, K., Sudhakar, C. & Ragu Prasath, A. Green synthesis and characterization of silver nanoparticles from sandalwood (Santalum album L.) extract for efficient catalytic reduction, antioxidant and antibacterial activity. *Biocatal. Agric. Biotechnol.* **57**, 103094. https://doi.org/10.1016/j.bcab.2024.103094 (2024).

Acknowledgements

The authors extend their appreciation to the Director, Amrita Vishwa Vidyapeetham, Mysuru Campus, for providing instrumentation and infrastructure facilities. The author acknowledges the SASIF, Kottayam, and Nano-mission Project "SR/NM/NS-20/2014" CNMS, JAIN, deemed to be a university, for providing instrumentation facilities. The authors extend their appreciation to the Ongoing Research Funding Program (ORF-2025-734), King Saud University, Riyadh, Saudi Arabia, for their support.

Author contributions

S.S.M., S.P.K.: Conceptualization, Methodology, Investigation, Formal analysis; S.S.M., R.K.B., B.K.D., P.S., P.B.S.S., K.S.A., C.S., S.P.K.: Data curation, Investigations, Formal analysis, Writing- Original draft preparation. M.I., R.G.A., V.S., E.S., S.P.K.: Visualization, Project administration, validation. S.P.K.: Resources, Supervision, Writing- Reviewing and Editing.

Declarations

Competing interests

The authors declare no competing interests.

Additional information

Supplementary Information The online version contains supplementary material available at https://doi.org/1

0.1038/s41598-025-32173-w.

Correspondence and requests for materials should be addressed to E.S. or S.P.K.